Journal of Sound and Vibration (2003) **259**(5), 1037–1065
doi:10.1006/jsvi.2002.5130, available online at http://www.idealibrary.com on IDEAL®

ACOUSTIC IDENTIFICATION OF COHERENT STRUCTURES IN A TURBULENT JET

G. Guj, M. Carley† and R. Camussi

Dipartimento di Ingegneria Meccanica e Industriale, Università di Roma Tre, Via della Vasca Navale 79, 00146 *Rome, Italy. E-mail: camussi@uniroma3.it*

AND

A. Ragni

Centro Italiano Ricerche Aerospaziali, (CIRA), Via Maiorise 1, 81043, *Capua (CE), Italy*

(*Received* 25 *November* 1999, *and in final form* 14 *January* 2002)

Fluid-dynamic events associated with noise generation in a subsonic jet are educed by conditioning in-flow velocity and pressure signals on farfield sound measurements. The jet is located in an anechoic chamber, and farfield noise measurements are performed simultaneously with in-flow anemometric and acoustic measurements at a number of distances x from the nozzle ($0 \leqslant x/D \leqslant 20$, with D the jet diameter). The experimental data are then analyzed with a conditional averaging procedure using peaks in the acoustic signal as a trigger. An analysis of the method is developed and supported by numerical simulations. The averaging procedure permits the identification of the average time signatures of in-flow velocity and pressure associated with noise-generating coherent structures in the flow, their position at the emitting instants and their temporal statistics. The physical properties of the events associated with the averaged time signatures are then discussed.

1. INTRODUCTION

1.1. BACKGROUND

The problem of noise generation by unsteady or turbulent jets has been of great interest since the introduction of the first aircraft jet engines about fifty years ago. The modern study of the problem began with the work of Lighthill [1], who developed a theory of noise generation by flows. The wave equation which incorporates the full non-linear laws of fluid motion and thus the aerodynamic sources, reads

$$\frac{\partial^2 \rho}{\partial t^2} - c^2 \nabla^2 \rho = \frac{\partial^2 T_{ij}}{\partial x_i \partial x_j}, \tag{1}$$

$$T_{ij} = \rho u_i u_j + (p - \rho c^2)\delta_{ij} - \text{viscous terms} \quad (\text{Lighthill tensor}). \tag{2}$$

Here the speed of sound is c, density and pressure perturbations are ρ and p, $\mathbf{u}$ the fluid velocity, $\mathbf{x}$ the spatial co-ordinate and t the time. This equation is valid within and without

† Visiting scholar, presently at Department of Mechanical Engineering, University of Bath, Bath BA2 7AY, England

0022-460X/02/$35.00

a source region, but outside a source, where linear acoustics is valid, the acoustic pressure can be found from the relation $p = c^2\rho$. Although the Lighthill theory has been remarkably successful in its application to noise generation by turbulence, of special interest for the present work are those formulations which employ vorticity as the primary aerodynamic variable. In these methods, especially in the case of low-speed flows, the flow field can be described very compactly in terms of its vorticity, making it convenient as a source term. In particular, in the works of Powell [2, 3], the source term of the wave equation is rewritten in terms of vorticity:

$$\nabla^2 p - \frac{1}{c^2}\frac{\partial^2 p}{\partial t^2} = -\rho_0 \nabla\cdot\left(\boldsymbol{\omega}\times\mathbf{u} + \nabla\frac{|\mathbf{u}|^2}{2}\right). \tag{3}$$

For a low Mach number flow in free space, the sound radiated to the far field is given by [4]

$$p(\mathbf{x}) = \frac{\rho_0}{12\pi c^2|\mathbf{x}|^3}\frac{\partial^3}{\partial t^3}\int\int\int_V (\mathbf{x}\cdot\mathbf{y})\mathbf{y}\cdot(\boldsymbol{\omega}\times\mathbf{x})\,\mathrm{d}^3\mathbf{y}. \tag{4}$$

As described in several previous works, equation (4) has a number of physical interpretations [3–6]. In these descriptions, the acoustic source can be related to the aerodynamics of the system since the farfield pressure is directly correlated with the time variations of the vorticity field via the third temporal derivative. These results are of great importance for the study of noise in subsonic jet flows in connection with the aerodynamic behavior and, in particular, the influence of large-scale coherent structures forming within the turbulent flow.

As clearly pointed out by Tam [7], in the case of cold subsonic jets, the instability waves are characterized by subsonic phase velocities and therefore, as demonstrated experimentally by Moore [8], are ineffective in producing noise. The crucial role in noise emission in cold subsonic jets is thus played by fine-grained turbulence [1] and by the coherent structures formed during the transition to self-similarity (see, among many references [9–12]). Indeed, it is well known that a vortical structure alone is insufficient for noise generation and radiation, several workers having indicated that the dominant noise generation mechanism should be interaction between large-scale vortices and, more precisely, vortex pairing (see, among many, the experimental work by Laufer *et al.* [13], the theoretical analysis of Ffowcs Williams and Kempton [14], and the numerical simulation of Verzicco *et al.* [15]). On the other hand, as suggested by Hussain [16] and Bridges and Hussain [17], for increasing Re (the Reynolds number based on the jet nozzle diameter D), the pairing of vortices becomes less frequent, and cannot be considered the dominant mechanism in noise generation. To clarify this aspect, experimental works were devoted to determine the spatial location of the acoustic sources. This task was pursued by using array processing techniques (e.g., by the polar correlation technique [18] or by the casuality method [19–22]), by acoustic mirrors [23], or by conditional averaging techniques based on in-flow measurements (e.g., references [24, 25]). However, these purely acoustic methods at best can give spectral information about the acoustic source without the possibility of giving a description of the aerodynamic structures which give rise to that source. Furthermore, results obtained so far do not precisely identify the region of noise emission (axial distances ranged from $3D$ to $10D$), rendering any correlation with the well-known fluid-dynamic phenomena which characterize the transitional process of the subsonic jet flow very difficult (see, e.g., the paper by Yule [11]).

Also from the purely aerodynamic viewpoint, the study of the unsteady quasi-deterministic coherent structures which characterize turbulent jet flows during the

transition to self-similarity has received great attention in the last years (see also the book by Lesieur [26]). Experimental analyses based on conditional averaging methodologies [27, 28]) have shown that at high Re, coherent structures are large-scale vortices characterized by a high degree of energy (and vorticity). Such structures are believed to be generated by shear layer destabilization and to have a ring-like shape, but, being intrinsically unstable far from the nozzle exit, their lifetime is very short [28, 19]. Furthermore, they are characterized by temporal and velocity gradient statistics which are strongly non-Gaussian due to their intermittent nature.

As indicated above, acoustic radiation is directly related to the temporal vorticity variations, and therefore efficient acoustic sources may be identified in those so-called *intermittent* structures which form within the jet flow past the end of the potential core. However, the role played by these structures in noise emission is still not clear. Indeed, experimental works conducted so far (see also references [30, 31]) do not give detailed information on the form of the vortical structures generating noise, as they do not yield a detailed time record of the acoustic source strength and do not give any indication on their spatial or temporal statistics.

1.2. OBJECTIVES OF THE PRESENT WORK

The main task of the present work is the analysis of the correlation between the dynamics of the unsteady intermittent structures forming in the transitional region of subsonic jet flows and the acoustic emission. As pointed out above, this aspect appears to be most relevant in the case of cold subsonic jets where the primary phenomenon responsible for noise generation has not yet been clearly identified, and is of importance in view of the possible strategies to be applied for noise control.

The issue of the present work is analyzed experimentally by the simultaneous measurements of the farfield pressure and in-flow pressure and velocity, and by the development of a conditional technique for ensemble averaging. With respect to previous approaches, the present procedure permits one to extract information regarding the spatial localization and the time statistics of the events associated to acoustic radiation. Furthermore, statistically averaged time signatures of the structures responsible for the farfield noise are obtained, giving some insights, even if qualitative, also on their topological properties.

The identification procedure here proposed and developed is based on the use of peaks in the farfield noise as a trigger. From the theoretical viewpoint, in the farfield noise approximation, it is implicitly assumed that propagation effects are neglected while only sound generation processes are retained. An out-of-flow microphone is used as a trigger for the conditional sampling of data obtained from an in-flow hot wire and/or microphone. Two aspects will then be developed:

- The triggering technique permits the localization of the region of the jet flow where most of the farfield pressure peaks are generated. This is done by analyzing the characteristic phase of the structures which result from the conditional average. If they are correlated with the *intermittent* structures described above, such a region should be localized where the jet flow is fully turbulent, sufficiently far from the nozzle exit.
- The technique allows tracking of the phase of the noise-producing events. In this way, it is possible to analyze their temporal statistics by computing the probability distribution functions (PDF) of the time delay between successive events. As shown in several previous works (e.g., references [32–35]), this is a powerful tool for determining whether the educed events have an intermittent character. Indeed, if the events generating noise

are intermittent in time and uncorrelated with each other, strongly non-Gaussian PDFs with exponential-like distributions are expected.

In order to support the present physical interpretation and results, the triggering method is modelled analytically and simulated numerically using a simple model representing the localized noise sources. Furthermore, the averaged time signatures obtained from the conditional technique are compared with similar ones obtained by a purely aerodynamic technique [29] which allows the retrieval of the signatures of the *intermittent* structures with no assumptions about noise generation or radiation.

The conditional averaging method is described in section 2, while an analysis of the method is presented in section 3. The experimental arrangements, measurement set-up and uncertainty evaluation, will be presented in section 4. In section 5, the results and main discussion are given, while section 6 contains some final remarks and the conclusions of the paper.

2. CONDITIONAL AVERAGING METHOD FOR STRUCTURE EDUCTION

The present conditioning method is similar to that proposed in reference [27], and it is based on the idea that coherent structures intensity variations, independent of their phase, generate large pressure fluctuations in the far field that can be used for triggering and selecting instants of noise emission.

We denote by $g(t)$ the signal to be averaged (velocity or inflow pressure) which is acquired simultaneously with the farfield pressure $p_o(t)$. In the procedure, a time point in $g(t)$ is selected as a trigger time t_0 if the second signal $p_o(t)$ has a peak at that position. The event selection is performed by fixing a threshold T, and considering time intervals corresponding to $p_o(t) \geqslant T$. Among all points, we therefore choose those satisfying the conditions

$$p_o(t) \geqslant T, \qquad \frac{\mathrm{d}p_o}{\mathrm{d}t} = 0, \qquad \frac{\mathrm{d}^2 p_o}{\mathrm{d}t^2} < 0. \tag{5}$$

The condition on the second derivative ensures that only time instants corresponding to the relative maxima of the function $p_o(t)$ are selected within the interval of $p_o(t)$ overcoming the threshold. Once the set of selected time instants is available, the velocity, pressure or both signals measured in flow are ensemble averaged to eliminate random fluctuations and educe the coherent contribution to the signal, should it exist. If the time signature of the noise-generating structures has a basic form in $g(t)$, this "template" is revealed by the averaged signal.

An interesting point is the possibility of individuating, statistically, the position where noise has been radiated. We can define Δt as the total time delay obtained as a difference between the time instant characterizing the averaged time signature (which can be deduced from its maximum) and the reference time corresponding to the peaks in the farfield pressure. On the basis of the averaging procedure, this reference time equals the acoustic time and may be set equal to zero if the sound propagation velocity (c) is assumed infinite. In particular, for $c = \infty$, three possibilities can be encountered: $\Delta t = 0$ for a noise emission at the same position as the in-flow probe, $\Delta t < 0$ for a noise emission downstream and $\Delta t > 0$ for a noise emission upstream. For finite c, the effect of the acoustic propagation is always a positive delay to be accounted for. Accounting also for the local convection velocity, which is evaluated by a proper aerodynamic characterization of the jet flow, and the measured Δt magnitude, it is therefore possible to retrieve the spatial location of the averaged noise source. We point out that the magnitude of the time delays and of their

spatial counterpart as extracted from the averaged structures plays a fundamental role in the interpretation of the results presented in section 5.

A further remark concerns the choice of the threshold level T in the event selection procedure. It has been verified that a change in T does not lead to a significant statistical change in the shape of the time signatures, in the magnitude of Δt and in the time statistics. However, a systematic study was performed to obtain the optimum value of T which maximizes the signal-to-noise ratio of the resulting averaged signals. It has been found that this condition leads to a value of T about 30% of the maximum value of the whole pressure signal. This is the configuration adopted in the post-processing procedure presented here.

3. A SIMPLE ANALYTICAL MODEL FOR VALIDATING THE EXPERIMENTAL ANALYSIS

In this section, a simple numerical analysis is used for reproducing the approach adopted in the conditional analysis of the experimental data. It is analyzed an "artificial" signal associated with a set of coherent structures generated at random initiation instants.

The objective of the simulation is to assess the capability of the farfield pressure conditioning to retrieve the shape of the averaged pressure induced by coherent structures on the in-flow signal even when a large intensity noise is added to the in-flow signal (thus simulating the actual background turbulence). The computational method is based on the use of standard routines for the numerical integration of the equations used for the computation of the acoustic pressure. It should be stressed that the reproduction of the details of the jet flow dynamics as well as of the actual coherent structures shape is not among the purposes of the simulation. Therefore, the model adopted for reproducing the acoustic strength of the structures is as simple as possible. Specifically, the procedure has been based on a model of the coherent structures as a train of line sources (see the book by Morse and Ingard [36, p. 772]). The line sources travel at constant velocity V_m over some length L; see Figure 1. For the purpose of the simulation, this model might be considered sufficiently accurate if jets of small radius are considered. In these cases, the actual wavelength of the structures is expected to be greater than the jet diameter, so that the source can be considered acoustically compact across its section. Obviously, this is not true along the axis of the jet, so that the source model must have some axial extent.

It is assumed that the shape of the structures, denoted as f_0, does not change over the length L which in a turbulent flow would correspond to the Taylor frozen turbulence hypothesis [37]. Furthermore, we assume that the structures arise at position $x = 0$ and break down at position $x = L$. This is valid if the source is monopole (radiates with spherically symmetric directivity) or if the change in directivity at the observer position does not change much as a function of source position x for $0 \leqslant x \leqslant L$. This is equivalent to saying that the angle subtended by the length L at the observer position is small, i.e., that the farfield approximation is valid. For a structure of acoustic source strength $f_0(x')$, which appears at position $x = 0$ at time τ_i, the acoustic source at position x on the jet, accounting for the Taylor hypothesis, is

$$f(x, t) = f_0(x - V_m(t - \tau_i)). \tag{6}$$

The sound $p(t)$ radiated to some point $\mathbf{x}_0$ is given by

$$p(\mathbf{x}_0, t) = \int_0^L \frac{1}{4\pi r} f_0(x - V_m(t - \tau_i - r/c))\, \mathrm{d}x. \tag{7}$$

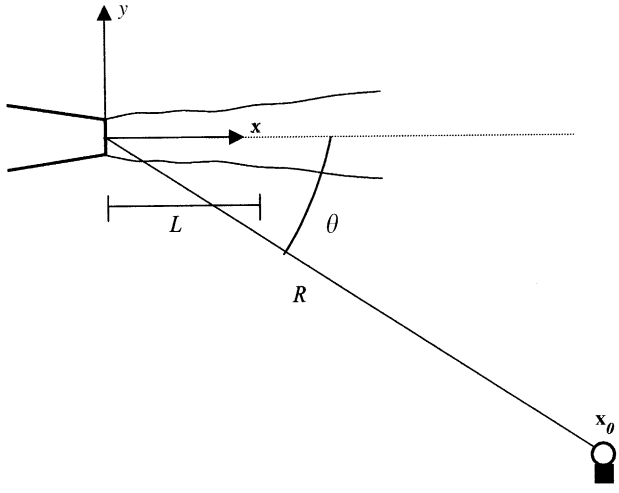

Figure 1. Line source model for coherent structure noise.

where $r = |\mathbf{x}_0 - \mathbf{x}|$. In the far field $1/r \approx 1/R$ and $r \approx R - x\cos\theta$, where $R = |\mathbf{x}_0|$ and θ is the angle of the observer subtended by the jet axis at $x = 0$. The radiated sound is then

$$p(\mathbf{x}_0, t) = \frac{1}{4\pi R}\int_0^L f_0(x(1 - M_0\cos\theta) + M_0 R - V_m(t - \tau_i))\,\mathrm{d}x, \tag{8}$$

where $M_0 = V_m/c$ is the jet Mach number. The total contribution from all structures f_0 released at times τ_i is then the summation and with a change of variable

$$p(\mathbf{x}_0, t) = \frac{1}{4\pi R(1 - M_0\cos\theta)}\sum_i \int_{M_0 R - V_m(t-\tau_i)}^{M_0 R - V_m(t-\tau_i) + L(1 - M_0\cos\theta)} f_0(x)\,\mathrm{d}x. \tag{9}$$

The location of peaks in the pressure time record is readily found by differentiating the previous equation

$$\frac{\mathrm{d}p}{\mathrm{d}t} = \frac{V_m}{4\pi R(1 - M_0\cos\theta)}\sum_i \{f_0(M_0 R - V_m[t - \tau_i] + L[1 - M_0\cos\theta]) - f_0(M_0 R - V_m[t - \tau_i])\} = 0, \tag{10}$$

so that it is clear that the position of peaks in the pressure time record for the noise radiated from the correlation length L is directly related to the form of the coherent structures (f_0) in the region of interest, and is a function of the "entry time" or "exit time" of structures τ_i. This result offers a possible mechanism for the relationship of the timing of pressure peaks to the timing of structures. It should be noted that in the present model, the structures in question are typically formed of vortex filaments, so that they have a small, but finite, axial extent and do not overlap. Furthermore, they dominate the source term during their passage [38], so that is can be assumed that at any point in the time series, only one structure contributes to the source.

This simple model shows that the presence of peaks in the farfield pressure is due to the entry (at $x = 0$) or exit (at $x = L$) of the structures sensed by the microphone. This means that the entry (exit) time may be interpreted as the instant of appearance (disappearance) of a structure which is advected by the local convection velocity during its lifetime. Therefore, the peaks in the farfield pressure may be attributed to structures which form

within the jet flow at the time instants τ_i, and which physically represent the *intermittent* structures in which we are interested (see also reference [14]).

We now specify the shape f_0 used to validate the conditional averaging technique. For the sake of simplicity, the model structure used was one period of a sinusoid, a form superficially similar to the known shape of the acoustic source associated with vortex interactions (see, e.g., reference [15]). The jet parameters were chosen to roughly represent the jet used in the experiments described in this paper. The structure wavelength was set equal to the jet exit diameter, D, and it has been assumed that such structures survive over a length $4D$. Release times for the structures were calculated as a sequence of random numbers from a uniform distribution which were sorted and scaled, so that the largest delay between structures was equal to one structure length divided by the mean flow velocity. This yielded a Poisson PDF for the time between structures, as shown in Figure 2(a) (see, e.g., the papers by Villermaux *et al.* [33] and Guj and Camussi [34]). A total of 10 000 structures were used, and the acoustic signal was calculated at a sampling rate of 40 kHz over a time period which contained all of the structure release times. This yielded 17 747 points for a record length of just over 0·44 s. The simulated microphone signal was calculated for $R = 10D$ and $\theta = \pi/6$ (in far field).

As a first check, the conditional sampling method described in section 2 was applied using a sequence of random trigger times, and, as expected, no "structure" on the in-flow averaged velocity was retrieved. Then, the procedure was applied using the farfield pressure for selecting the trigger times. Figure 2(b) shows part of the simulated pressure signal where the positions of the peaks and troughs are evidenced, and Figure 3 shows the result of applying the conditioning procedure to the simulated signals based on the peaks of Figure 2(b). The recovered structure is shown with the genuine structure superimposed for comparison. The identified shape represents accurately the known form of the source even if there is some noise in the region outside the structure proper as an effect of statistical convergence.

The effect of random noise (or noise from other source regions) on the procedure has been examined by introducing spurious peaks in the simulated microphone signal by the addition of a Gaussian signal of amplitude equal to 5, 10 and 100% of the r.m.s. "microphone signal" amplitude. The resulting educed structures are shown in Figure 4, with the 0% noise structure shown for comparison. The addition of noise has the effect of smoothing the educed structure and lowering the noise floor due both to errors introduced in the position of acoustic peaks and the increase in number of non-structure peaks. The basic shape and phase of the structure are, however, well recovered even for the case of highest noise level, thus showing the robustness of the proposed conditional procedure.

Two final points are of some interest in examining the experimental results to be presented later. The first is that for a given sequence of structure generation times, the acoustic signal is the same, the trigger times do not change and the same source will always be educed. The time delay of this source will depend, however, on the probe position. Figure 5 shows the sources educed with the probe signal simulated for three different values of x. Since the probe always sees the same time record, but with a temporal shift which depends on its position, the change in delay with probe position can be taken as an indication of the initiation point of the structure.

Secondly, equation (10) has two sets of solutions yielding the pressure peaks: any given structure will be seen twice (entry and exit times) if a long enough sample length is used. This feature was not exploited in the experimental processing but can be seen in the simulated data, Figure 6. A second source is educed with a separation between the two sources which depends on the parameters L, V_m and θ.

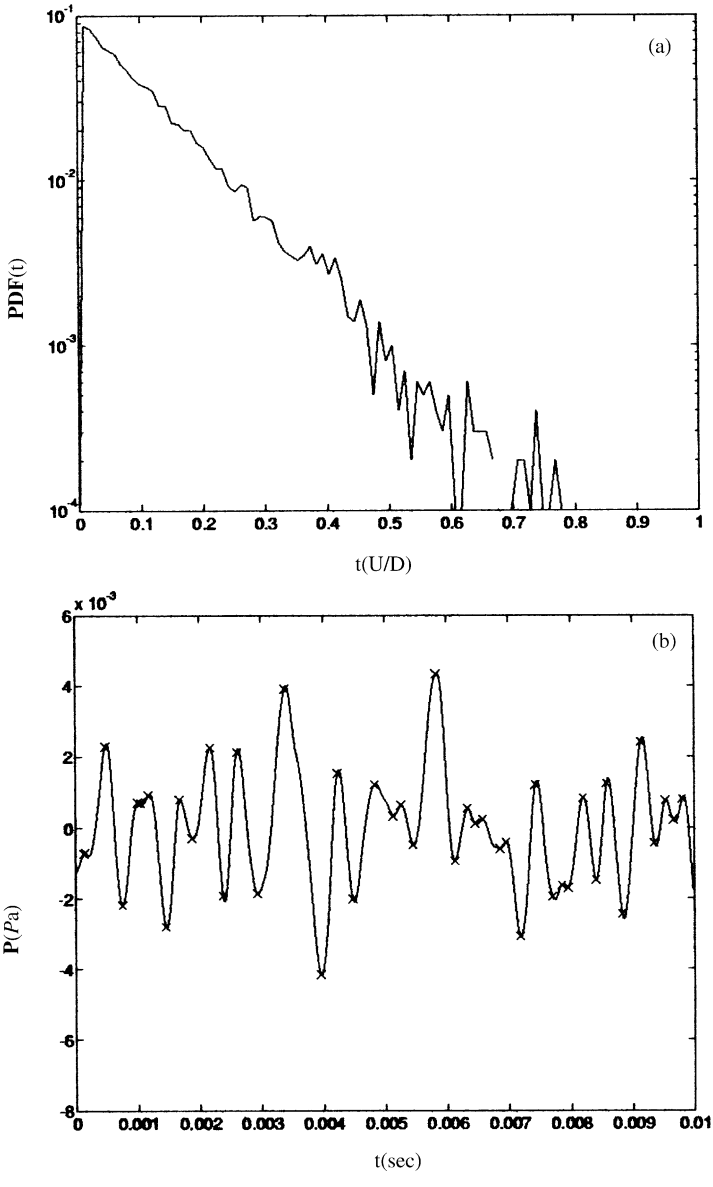

Figure 2. Simulated signal characteristics: (a) PDF of time between structures versus $\Delta\tau u/D$; (b) pressure signal (solid line) and predicted peaks ("x").

4. EXPERIMENTAL SET-UP AND UNCERTAINTY EVALUATION

4.1. EXPERIMENTAL FACILITY AND APPARATUS

Experiments were carried out inside the anechoic chamber available at the "Agenti Fisici" laboratory of Italian National Institute of Occupational Health and Safety (ISPESL). The chamber is characterized by a minimum size of 3·6 m and acoustic absorption greater than 99%. The walls (including roof and floor) are covered with insulating panels and wedges of length 75 cm (the minimum cut-off frequency is 115 Hz

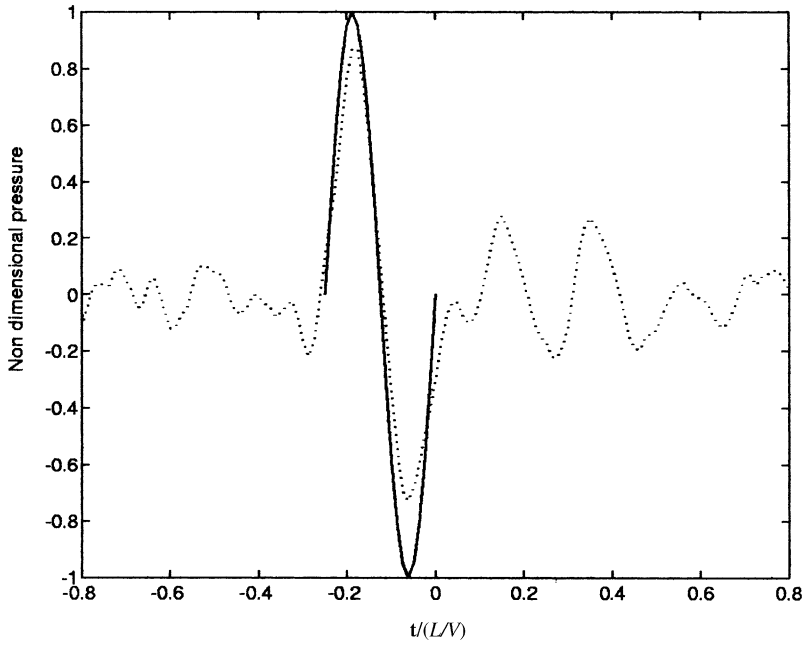

Figure 3. Identified and "actual" structures, identified shown as dotted line, "actual" as solid line.

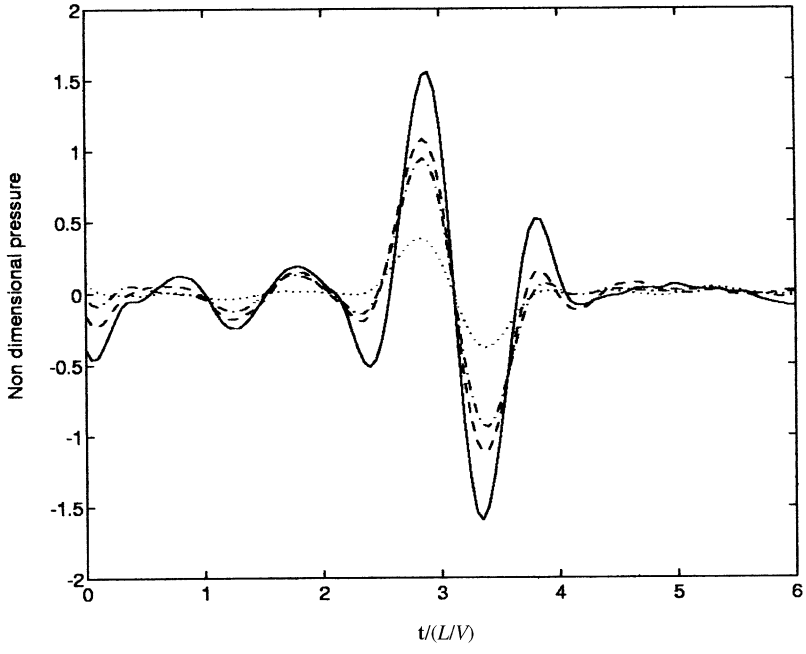

Figure 4. Noise effect on educed structure. Structure for 0% added noise shown as solid line, 5% dashed, 10% dash-dotted line and 100% dotted line.

and the reverberation time of the chamber is less than 10^{-1} s). The jet was mounted on a support and connected to the fan by a channel of length 8 m, so that the fan could be kept outside the anechoic chamber and would not affect the measured acoustics. The fan was

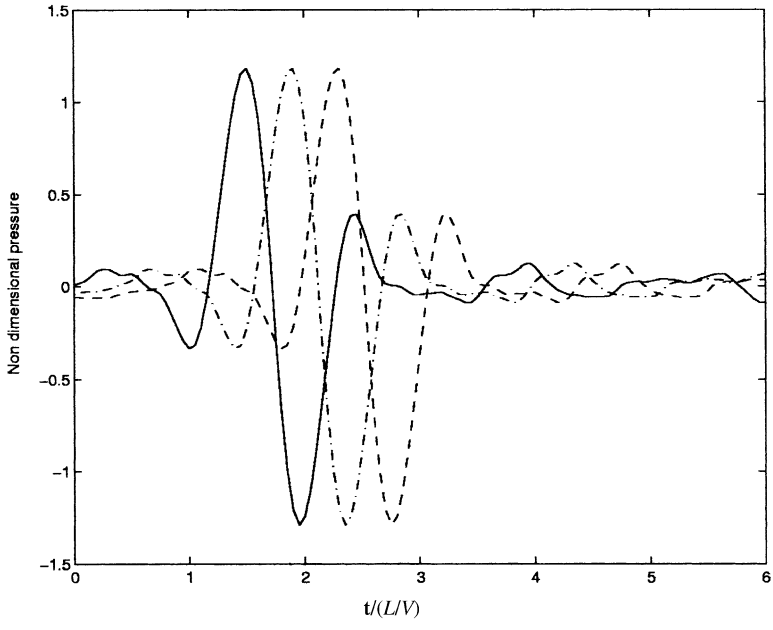

Figure 5. Sources educed with the probe signal simulated for three different values of x (probe position).

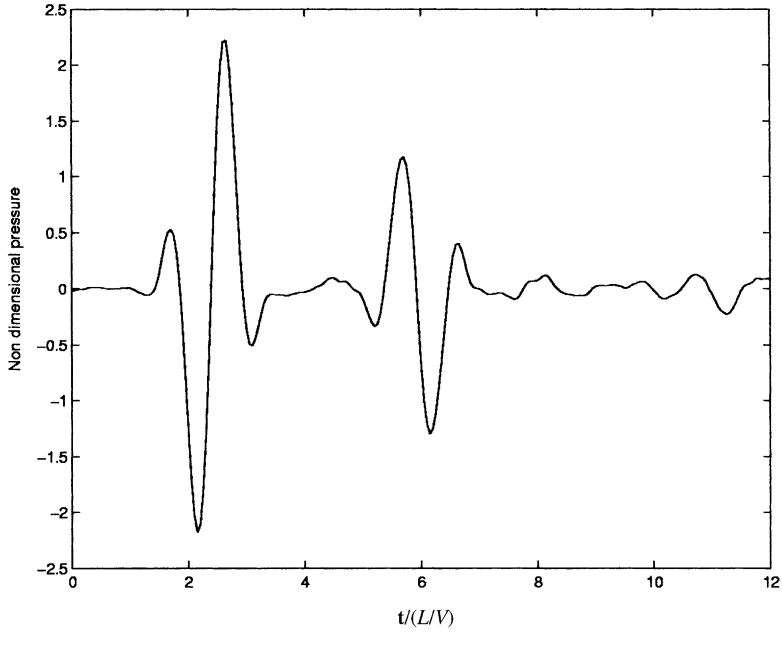

Figure 6. Signature of two structures as a consequence of the two sets of solutions of equation (9).

isolated from the jet by means of rubber joints and nozzle vibration was found to be negligible. A sketch of the experimental set-up is reported in Figure 7.

A jet with a circular nozzle of diameter 25·6 mm was used. The nozzle was fitted with a honeycombed channel and a series of screens for turbulence control. For all

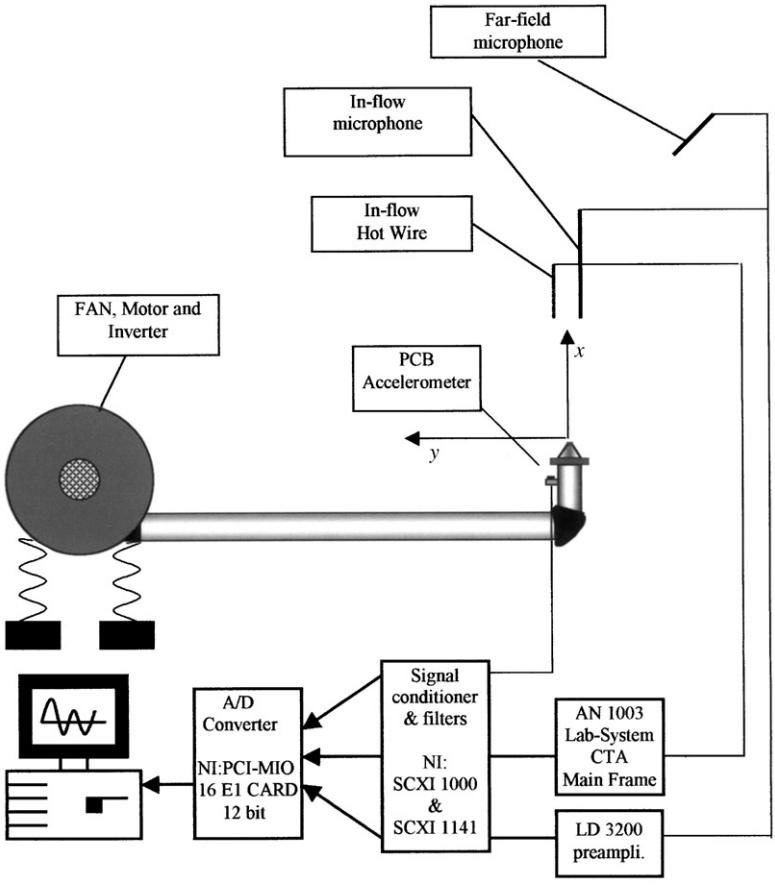

Figure 7. Experimental arrangement and probe positioning.

measurements, the mean velocity at the jet exhaust, U_0, was fixed at about 80 m/s. This corresponds at the nozzle exit to $\mathrm{Re} \simeq 1{\cdot}4 \times 10^5$ and $M \simeq 0{\cdot}23$. Taking into account that M decreases for increasing distances from the nozzle, the flow is subsonic and, as pointed out above, the velocity of sound may be considered infinite in comparison to the convection velocity.

4.2. INSTRUMENTATION AND SET-UP

The pressure and velocity signals were acquired using a 12 bit A/D converter, connected to a signal conditioner and digital filters, with a cut-off frequency of 20 kHz and a minimum roll-off to 48 dB/octave. Simultaneous velocity, pressure and acceleration (for vibration monitoring) data were acquired at a sampling frequency $F_s = 40$ kHz per channel. For both pressure and velocity signals, the number of samples acquired was 6×10^5 per channel, which ensures good statistical reliability for the averaging procedures.

The microphone equipment consisted of a Brüel & Kjaer 4135 microphone (1/4 in) for farfield measurements, and a Brüel & Kjaer 4138 microphone (1/8 in) with a nose-cone for in-flow measurements.

The microphones were fitted with Larson–Davis preamplifiers connected to a four channel Larson-Davis 3200 Spectrum Analyzer. Microphones were calibrated using a Brüel & Kjaer 4228 Pistonphone with a sound pressure level (*SPL*) of 124 dB at 250 Hz.

The hot wire anemometry (HWA) measurements were performed with a "gold-plated" 90° single probe of sensitivity length 1 mm (type 55P11 by DANTEC) connected to a constant temperature anemometer (CTA) module and mainframe AN-1003 by *Lab-System*. Both the anemometer and the in-flow microphone were fixed on the same support about 1 cm apart. It has been checked that this configuration minimizes the reciprocal interference. A block diagram of the instrumentation was also reported in Figure 7.

Hereafter, we denote the non-dimensional radial co-ordinate by y/D and the axial co-ordinate by x/D (Figure 7). Preliminary acoustic measurements were conducted in the anechoic chamber to estimate and minimize the influence of the in-flow probes on the pressure signals and more details are presented in section 4.4. Also, in each flow configuration the out-of-flow microphone axis was rotated (from 20 up to 90° with respect to the jet axis) in order to achieve the largest sensitivity in each case. In agreement with the results of Shaffar [23] and Ribner [39], and taking into account the directivity of the adopted microphone, it was found that the best orientation corresponds to an angle of about 30°. This angle between the out-of-flow microphone axis and the HWA probe location (taking as axial reference the jet axis) was maintained during all measurements. In order to maintain a farfield condition, the distance between the out-of-flow microphone and the jet axis was varied in the range $4 \leqslant y/D \leqslant 18$.

Hot wire and eventual pressure measurements were taken at several values of x/D within the flow ($0 \leqslant x/D \leqslant 22$), with $y/D = 0$ in all cases. It was verified that in all of the selected positions no flow reversal was observed and that the relative turbulence level (RTL) was always lower than 25%. These conditions ensured the validity of using HWA and of adopting the Taylor hypothesis to exchange time and space [37].

We finally point out that the aim of installing, in some of the measurements performed, the in-flow microphone together with the anemometric probe was mainly to assess and have confirmation of the reliability of the results concerning the eduction of averaged shape and the magnitude of the time delays, as discussed in the next section. As will be shown in section 4.4, in-flow pressure measurements are also used to quantify the uncertainties related to disturbances produced by the in-flow probes.

4.3. AERODYNAMIC QUALIFICATION OF THE JET FLOW

The jet flow was characterized using preliminary HWA measurements. In particular, the initial boundary layer was checked to be laminar and the mean velocity and standard deviation profiles at different distances from the nozzle exit were measured for different mean axial velocities. The flow at the nozzle exit was found to be characterized by a low turbulence level ($\simeq$1%) and the mean velocity having a top hat profile. Furthermore, it has been verified that the mean velocity and standard deviation variations with distance from the nozzle exit were in agreement with the expected laws (see, e.g., the paper by Wygnanski and Fiedler [40]). The values of the mean velocity measured at the jet axis for increasing x/D are reported in Table 1.

Measurements of statistical properties along the jet axis (longitudinal velocity standard deviation, skewness and flatness) have shown that the potential core ends at about $5D$. After about $8D$ the velocity profiles show similarity with the typical shape (see also the book by Schlichting [41]). From the momentum conservation law, it was possible to

TABLE 1

Mean velocity measured at the jet axis as a function of x/D

x/D	U_0 (m/s)
0	81·8
2	80·3
4	77·4
6	53·2
8	40·2
10	31·7
12	26·4
14	21·7
16	19·8
18	17·6
20	16·5

calculate the momentum thickness, $K = 2\pi \int_0^\infty U^2 y \, dy$ which, for $x/D = 8$, was $0{\cdot}24\,m^4/s^2$. Examples of the aerodynamic qualification results are given in Figure 8, where we report the velocity and standard deviation profiles measured at the nozzle exit. Under the same flow conditions, for further validation, a spectral analysis was performed of the velocity signals acquired on the jet axis. Analysis of the energy spectra in the region close to the nozzle showed an energy peak at a frequency corresponding to a Strouhal number $St = fD/U_0 \simeq 0{\cdot}5$ that is typical of round jets as the preferred Strouhal number of the jet prevailing near the end of the potential core (see the review by Cantwell [42]). This result was confirmed for different exhaust velocities. On the other hand, in the region far from the nozzle exit (about $x/D \geqslant 8$), a spectrum with an $f^{-5/3}$ power law has been observed, indicative of a fully turbulent flow [37]. This means that for about $x/D \geqslant 8$ the flow has reached a condition of fully developed turbulence. Examples of energy spectra are shown in Figure 9 for $x/D = 2$ and 12, with the $f^{-5/3}$ line indicated in Figure 9(b).

4.4. MEASUREMENT ERRORS

The main source of uncertainty affecting the results presented in the following section can be associated to the presence of the in-flow probes (the hot wire, the microphone or both) which, being intrusive, interact with the main stream and its fluid structures and surely generate undesired noise and flow disturbances. Indeed, the flow structures might interact with the solid probes and may produce both periodic and (non-periodic) random pressure fluctuations both in-flow and in the far field. These aspects are analyzed based on *adhoc* measurements of the farfield pressure performed in several flow conditions with and without the in-flow probes or (with reference to the scheme of Figure 7) by eliminating only one of the two in-flow probes.

As a first qualitative example, a comparison between a segment of the farfield pressure signal measured in the presence of both the in-flow probes at $x/D = 12$ and the corresponding signal obtained for the same flow conditions, but without the in-flow probes, is reported in Figure 10. A qualitative analysis shows that no significant variations of the peaks separation as well as of the pressure fluctuation amplitude can be observed, thus indicating that in-flow probe noise effects are not relevant.

A more quantitative comparison can be achieved by the analysis of the farfield pressure spectra (*PS*) with and without the intrusive probes. The farfield *PS* obtained at $x/D = 12$

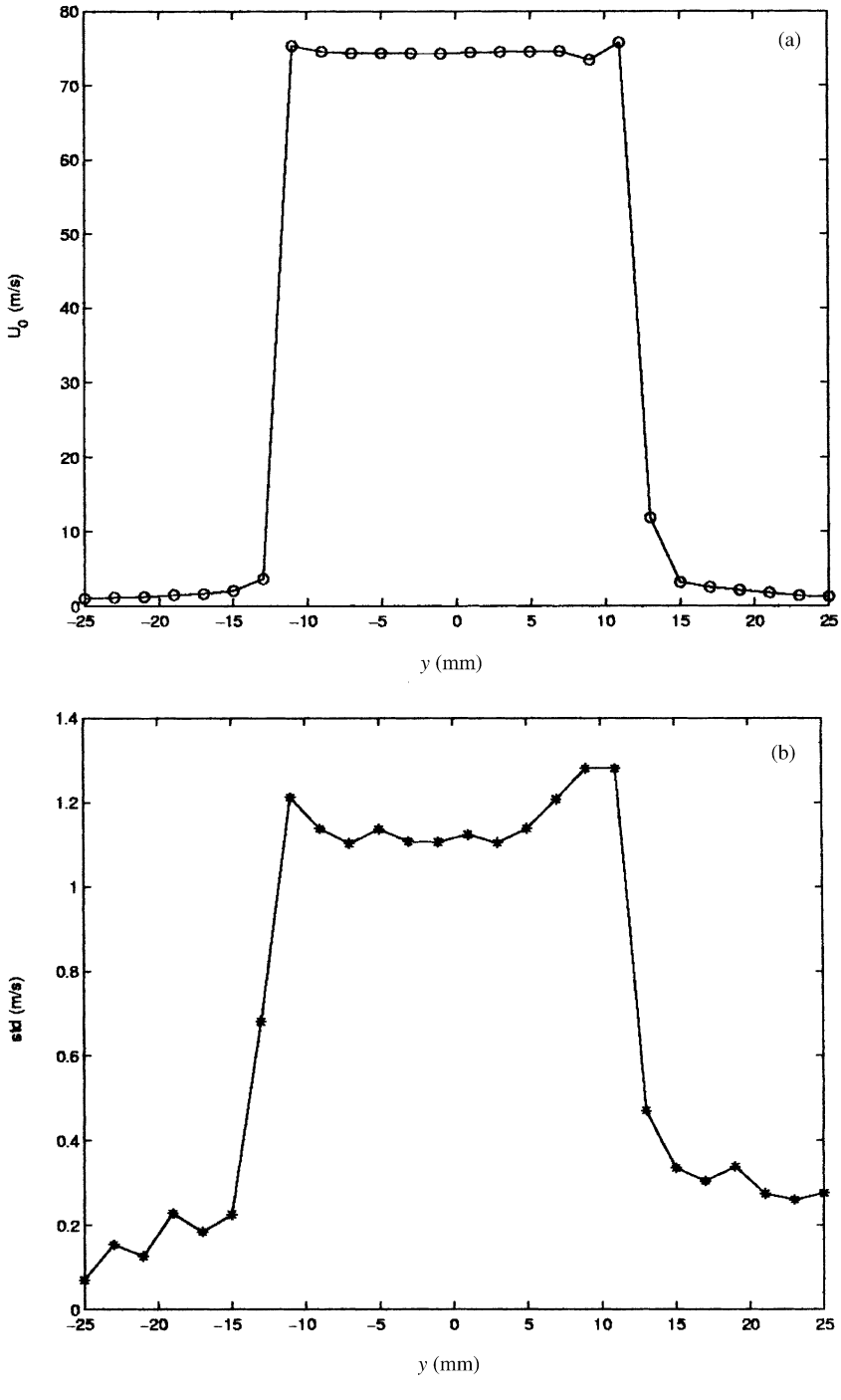

Figure 8. Mean velocity (a) and standard deviation (b) profiles at the nozzle exit.

and corresponding to the signals reported in Figure 10 are presented in Figure 11. It is shown that only negligible differences can be observed for frequencies larger than about 500 Hz.

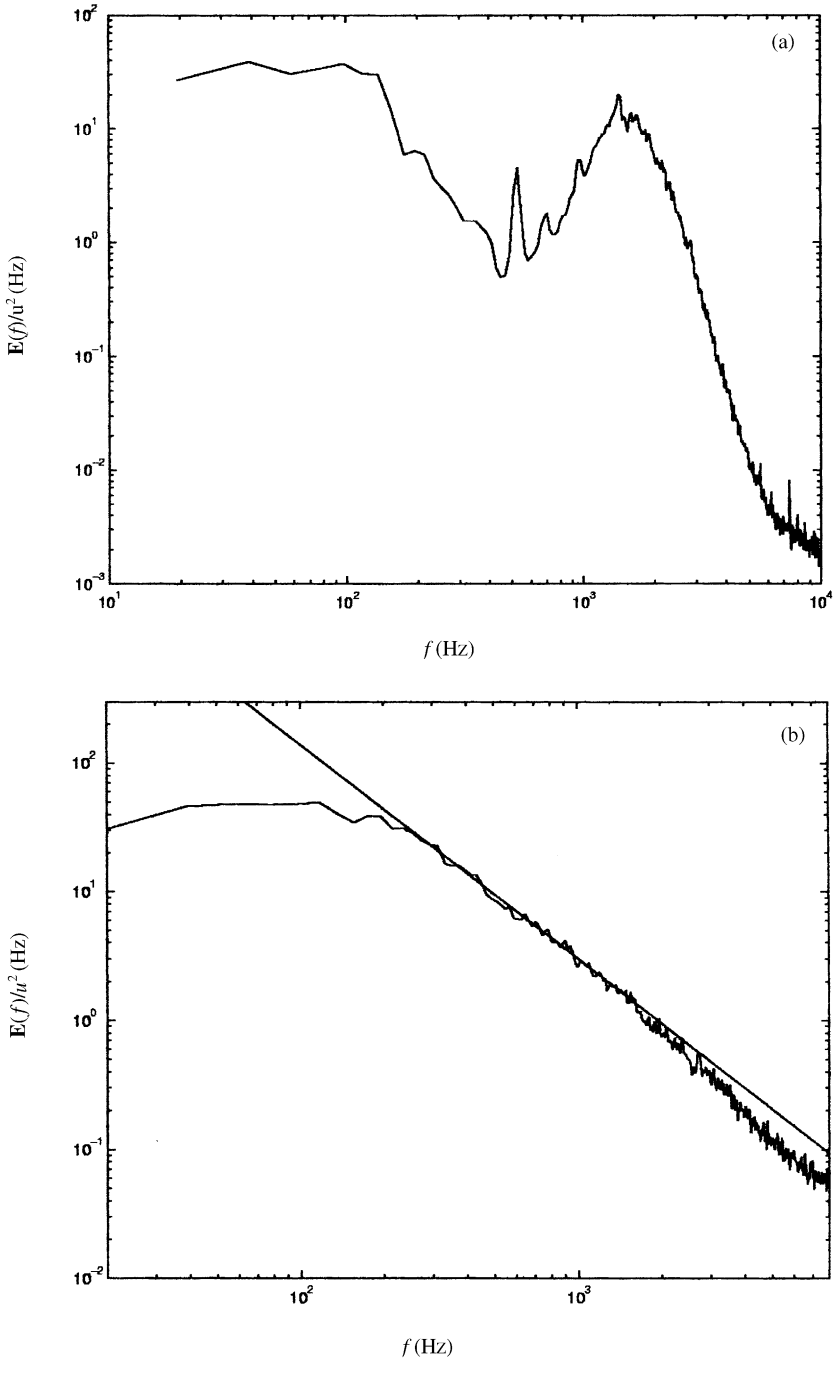

Figure 9. Energy spectrum for (a) $x/D = 2$ and (b) $x/D = 12$. The straight line in (b) indicates the Kolmogorov $f^{-5/3}$ scaling law.

A more precise estimation of the global effects of the in-flow probes has been performed by computing the overall farfield *SPL* for several distances from the nozzle exit. The summary of the results is presented in Table 2, where the relative difference between the

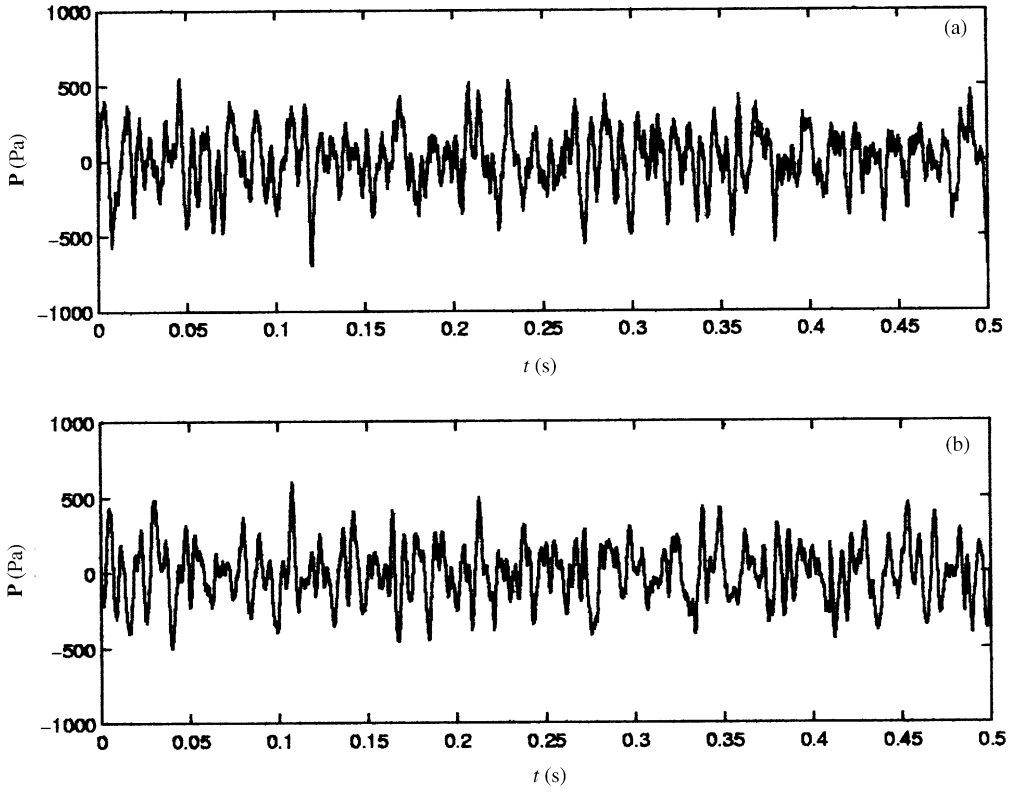

Figure 10. Examples of farfield pressure time series acquired without in-flow probes (case (a)) and with in-flow probes located at $x/D = 12$ (case (b)).

overall *SPL* measured with and without the in-flow probes is reported as a function of the non-dimensional distance *x*/*D*. It is shown that the largest error is observed for the position closest to the nozzle exist. This behavior may be attributed to the periodic nature of the velocity fluctuations in the near region, which can lead to more efficient structural excitations of the solid probes. In any case, the relative amplitude of such an effect never overcomes 4%, and thus it can be safely neglected.

We underline that the analysis of *PS*, or *SPL*, can give useful information only on the effect of periodic or long-time duration signals since unsteady and time-localized effects cannot be efficiently retrieved by the Fourier decomposition. The random noise emitted by the in-flow probes anyway may affect the averaged time signatures, and so the presented results, because it influences directly the phase of the farfield pressure peaks used for the conditional averaging. In order to clarify this point, specific measurements of in-flow acoustic pressure conditioned on the farfield pressure have been performed with or without the presence of the in-flow hot wire probe. This analysis therefore is needed to clarify in which amount the in-flow hot wire probe affects the averaged time signature of the in-flow pressure. An example is reported in Figure 12 showing that the averaged signature is not modified by the presence of the other intrusive probe, for what concerns its shape, amplitude, time delay and even the background noise. Similar results have been obtained in other positions confirming that no significant distortion is observed on the averaged signatures as an effect of the in-flow probes acoustic disturbances.

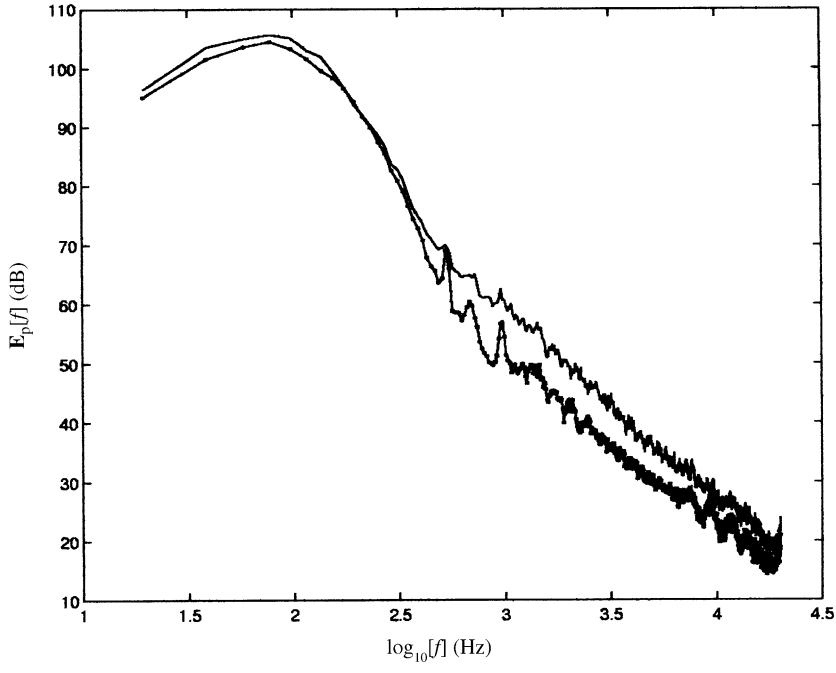

Figure 11. Examples of farfield pressure spectra corresponding to the time series of the previous figure. Solid line corresponds to the signal with in-flow probes located at $x/D = 12$, solid–dotted line to the signal without in-flow probes.

TABLE 2

Relative difference between the farfield SPL measured with (SLP_w) and without (SPL_{wo}) in-flow probes; ΔSPL is thus defined as $|SPL_w - SPL_{wo}|/SPL_w \times 100$

x/D	ΔSPL (%)
3	3·96
6	1·46
9	0·03
12	0·4

Finally, it should be stressed that (see section 5) the presence of a time delay in the time signatures of the averaged structures reported in Figures 13–16 of section 5 indicates that the peaks in the farfield pressure are (statistically) associated to events which are located at positions different from the location of the in-flow probes: upstream the in-flow probes location for negative time delay (Figures 13(a), 13(b) and 14(a), 14(b)) or downstream for positive time delay (as qualitatively shown in Figure 16). Bearing in mind the interpretation of the time delay, given in section 2, it is straightforward to conclude that the averaged time signatures are averaged contributions of noise-emitting structures, while the absence of any structure with zero time delay demonstrates that the in-flow probe noise is negligible or is statistically uncorrelated with the farfield pressure peaks. Another possible source of disturbances is the fluid dynamic structures interactions with the probe supports at a distance downstream of the sensing sections. However, this feature is not

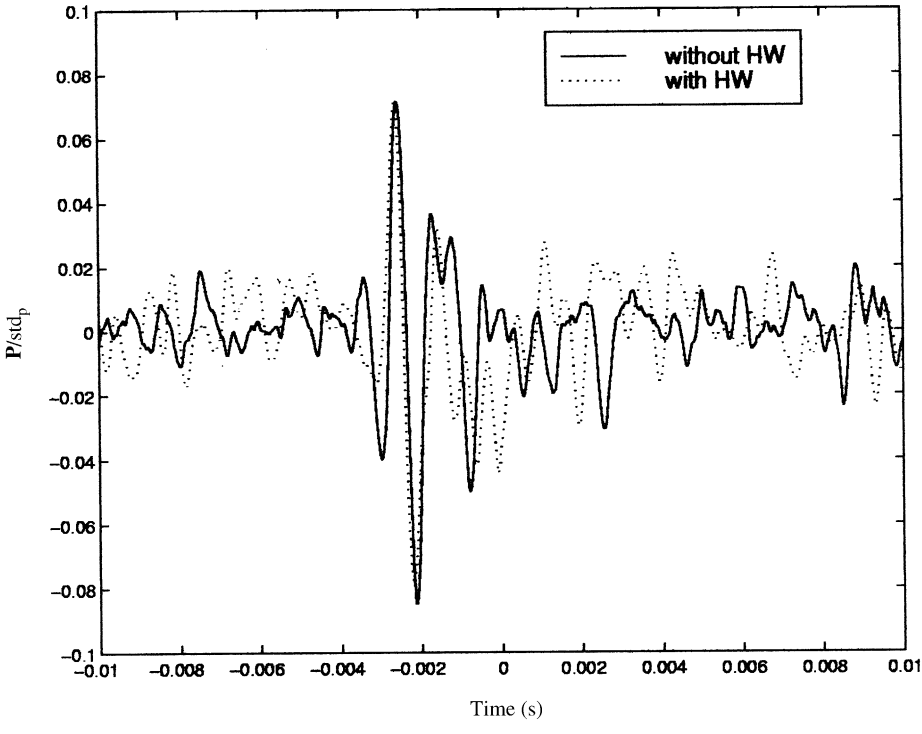

Figure 12. Comparison between the averaged time history of the in-flow pressure at $x/D = 2$ obtained from the in-flow pressure signal with and without the hot wire installed within the flow. std_p is the pressure standard deviation.

compatible with the negative time delay observed in Figures 13 and 14 which instead indicates that events emitting noise are located upstream of the probe's location and not downstream.

In summary, it has been clarified that the disturbances due to the presence of the inflow probes do not affect significantly the global spectral features as well as the averaged time signatures. It can be argued that their only relevant effect is the degradation of the statistical convergence of the averaging procedure. The elimination of such undesired effects can therefore be useful to obtain larger signal-to-noise ratio averaged structures with a number of averages relatively smaller than those performed in the present analysis.

5. RESULTS

In this section results obtained for the educed structures are presented. The velocity and pressure averaged data are non-dimensionalized on the standard deviation of the signal. A comparison with a reference aerodynamic coherent structure identification technique [29] is also presented as well as an analysis of the time delay statistics.

5.1. AVERAGED TIME SIGNATURES

In Figure 13 the structure educed for $x/D = 2$ is presented in terms of the averaged velocity. This result is representative of the behavior observed in the range $0 \leqslant x/D \leqslant 4$. We observe two effects at different frequencies. The first corresponds to quasi-periodic

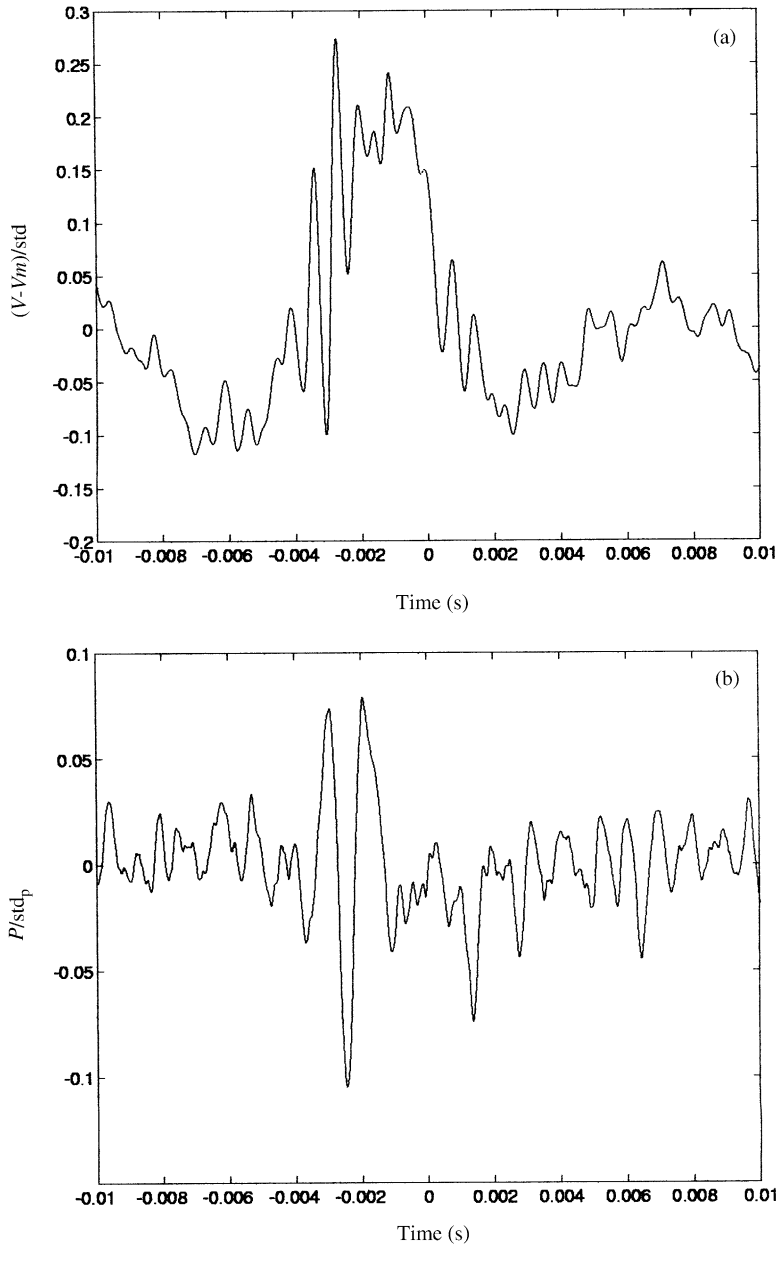

Figure 13. Averaged in-flow time histories conditioned on the farfield acoustic pressure, $x/D = 2$: (a) velocity; (b) pressure. The local mean velocity is denoted as V_m.

oscillations with a frequency coinciding with that of the energy peak observed in Figure 9(a). It may therefore be interpreted as induced mostly by oscillation of the shear layer, a common feature in subsonic jets in the mixing region near the nozzle exit. Figure 13(a) also reveals that these oscillations are superimposed on a lower frequency structure. It appears to be induced by a large-scale structure which has a peak at a negative time. Since this is a velocity induced by a fluid-dynamic event advected by the mean

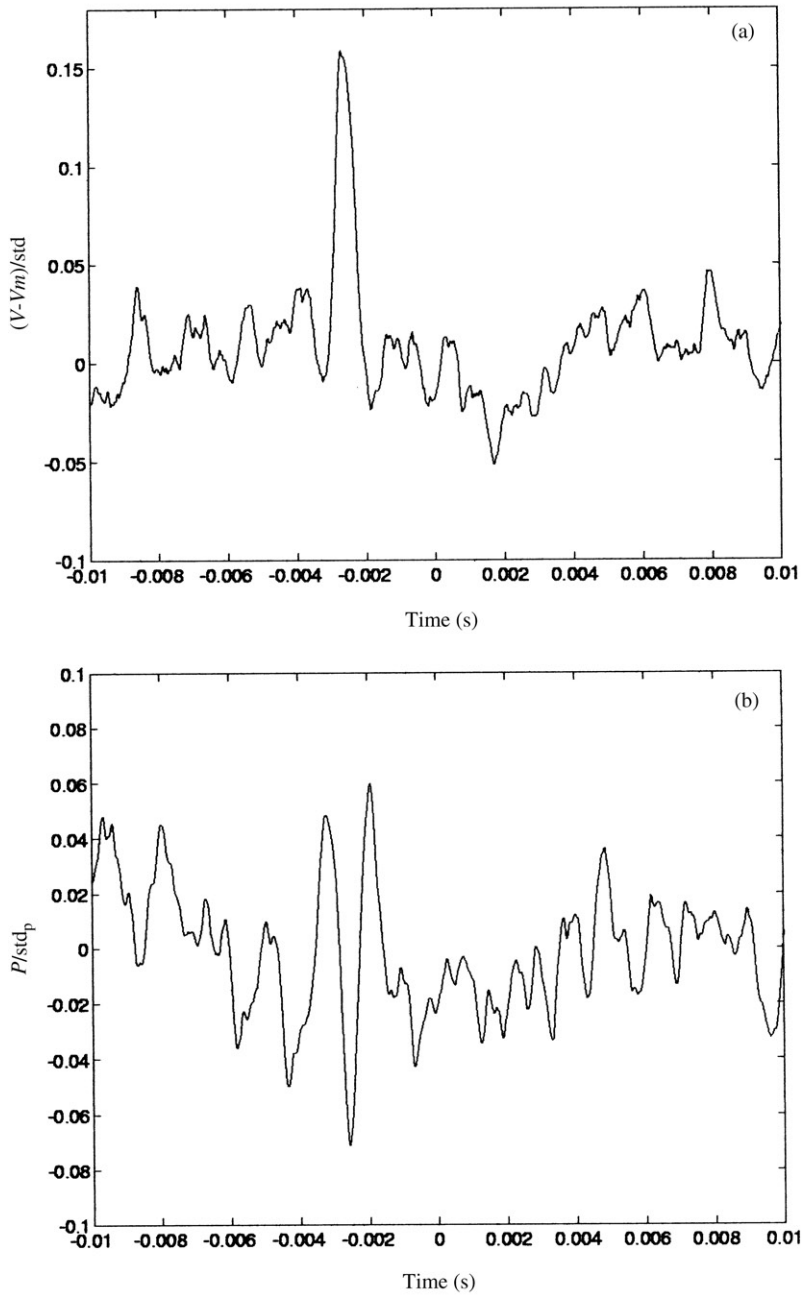

Figure 14. Averaged in-flow time histories conditioned on the farfield acoustic pressure, $x/D = 6$: (a) velocity; (b) pressure.

convection velocity, the time corresponding to the maximum may be associated with the instant of passage of such a structure through the anemometric probe. As pointed out above, the negative Δt observed in Figure 13(a) indicates that the structure, whatever it is, has emitted noise after passing through the in-flow probe position. This is also confirmed by analysis of the averaged in-flow pressure (Figure 13(b)). Here, the dominant effect is the

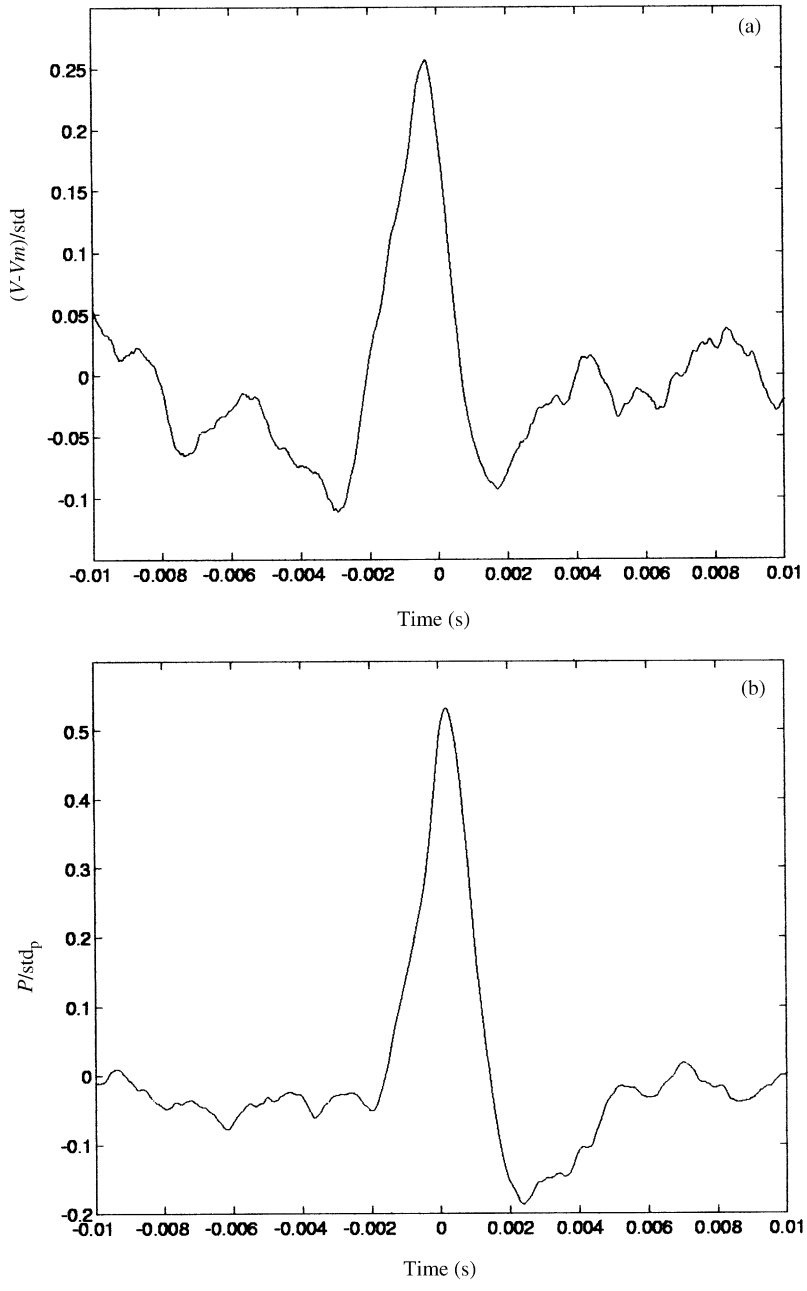

Figure 15. Averaged in-flow time histories conditioned on the farfield acoustic pressure, $x/D = 9$: (a) velocity; (b) pressure.

high-frequency oscillation related to the shear layer instability but, again, a negative time delay $\Delta t < 0$ may be observed, with the same magnitude as in the case of the averaged velocity. Similar results are obtained for $3 \leqslant x/D \leqslant 4$ and are not reported for brevity.

The above results indicate that the farfield radiated noise is actually strongly affected by events belonging to the fully developed region of the jet flow. More precisely, accounting

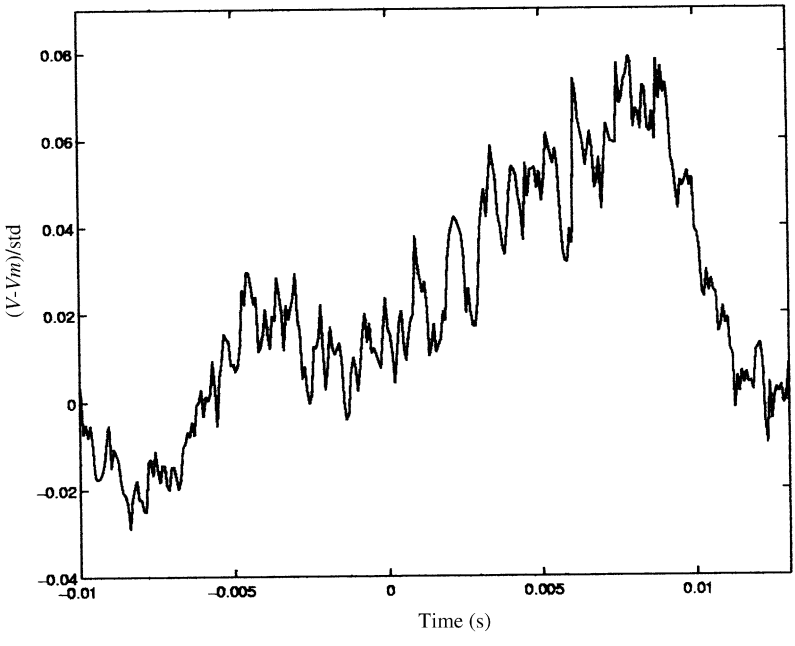

Figure 16. Averaged in-flow velocity time history conditioned on the farfield acoustic pressure, $x/D = 20$.

for the local value of the convection velocity (see Table 1), the sound speed (343 m/s) and the inflow–outflow probes distance, it is possible to calculate the time shift Δt of the low-frequency events in terms of space length. For example, in the case of Figure 13(a), the probes are located at $x/D = 2$ and their distance from the out-of-flow probe is $11D$; thus, the total negative time delay is $-0{\cdot}0022$ s ($-0{\cdot}003$ s being the advective time delay and $0{\cdot}0008$ s the sound propagation delay). The local measured convection velocity is $80{\cdot}3$ m/s, so that the peak in Figure 13 is due to some event, which assuming a constant convection velocity, is located at $0{\cdot}177$ m downstream of the probe location, i.e., at $x/D \simeq 8{\cdot}9D$ from the nozzle exit. If we account for the reduction of the convection velocity from $x/D = 2$ downstream, the more accurate spatial location of the noise-emitting event is $x/D \simeq 7{\cdot}2$. At the position $x/D = 6$, the time delay magnitude decreases as is shown in Figure 14(a, b), where an advective time delay of approximately $-0{\cdot}0025$ is observed both in terms of velocity and, even if with a lower signal-to-noise ratio, in terms of pressure. At $x/D = 6$, the spatial location of the noise-emitting event is $x/D \simeq 8{\cdot}9$ for a local convection velocity of about 53 m/s and $x/D \simeq 8{\cdot}5$ accounting for the deceleration of the mean convection velocity at larger x/D. Therefore, the two examined positions of the hot wire probe yield the location of the sound-emitting structures within the range $7{\cdot}2-8{\cdot}5D$.

The low-frequency effect becomes dominant for both the in-flow velocity and pressure, at positions $x/D > 6$. Such a behavior is partially related to a moving average effect due to the jitter in the window, i.e., due to possible error in the position of genuine peaks in the acoustic time record. The strength of this effect will depend on the size of the error in the peak position. From Figure 4, however, it was shown that even when the r.m.s. value of the added noise was 100% of the true signal, the educed structure retained the form of the original, with no obvious distortion in the shape. It can be argued therefore that the

disappearance of the high-frequency oscillations for large x/D is the physical effect related to the well-known disappearance of periodic structures for $x/D \simeq 6-8$.

What is of interest for present purposes is that by moving the in-flow probe to greater values of x/D, the time delay still decreases, reaches zero and then increases to positive values, thus revealing that the position of the events emitting noise remains about constant. As an example, the results obtained at $x/D = 9$ are reported in Figure 15. It is shown that the advective time delay is now very close to zero, thus confirming that the noise-emitting region should be very close to their location. Also we have to observe the high level of the amplitude of the averaged signals which corresponds to 25 and 50% of the standard deviation of the velocity, and the pressure respectively.

Further downstream, for the probe's position $x/D > 9$, the advective time delay is observed to become positive and to increase in magnitude. It should also be stressed that for increasing x/D, the averaged in-flow pressure becomes less significant, due to the lower signal-to-noise ratio as the flow becomes fully turbulent. An example of the far region result is reported in Figure 16 corresponding to $x/D = 20$. Even if with a lower signal-to-noise ratio, it gives a clear indication of a positive advective time delay which corresponds to noise emission that happens in space before the event reaches the in-flow probes. The spatial location of the noise emission, accounting for the decelerating convection velocity and the sound propagation speed, corresponds to a position of about $x/D \simeq 8$, but this result, due to the lack of statistical convergence, is only qualitative. It should be stressed that the larger value of the background noise at large x/D supports the idea that the structures which emit noise have a short lifetime. Indeed, since they generate noise at about $x/D \simeq 8$, only few of them conserve a coherence in shape up to $20D$, and, due to the high turbulence level, the velocity they induce is almost completely covered by the random fluctuations. This explains why, at large distances from the region where the farfield pressure peaks are generated, the averaging procedure leads to very disturbed signals. A better statistical convergence would be obtained by acquiring a much larger number of samples in order to significantly increase the number of averages.

5.2. COMPARISON WITH A REFERENCE IDENTIFICATION TECHNIQUE

In order to further validate the above presented results, and to give some, at least qualitative, indication of the physical nature of the noise-generating events, an alternative coherent structure identification technique has been applied to the anemometric data, without using the acoustic signals. The technique adopted is that recently proposed by Camussi and Guj [29] which has already been applied to a turbulent jet flow [28]. The choice of this procedure has been dictated by the possibility of educing coherent structure time signatures even when the flow is very turbulent. We note only that the identification procedure (hereafter called the *wavelet* method) is based on a wavelet transform of the velocity signals and on an ensemble averaging procedure conditioned on local energy bursts. It has been shown [29] that structures educed by this methodology are those responsible for turbulence intermittency. Indeed, if events educed by this technique are removed from the original signal, the velocity gradients show a Gaussian statistic and the effects of turbulence intermittency are no longer observed [34]. A comparison between results obtained with the *wavelet* and acoustic methods may therefore help in understanding if structures responsible for intermittency are correlated with the events educed by the far-field pressure conditioning, presently proposed.

In Figure 17, the results obtained at $x/D = 3$ and 10 with the *wavelet* method are presented. A time delay is not present in this case due to the application of a phasing

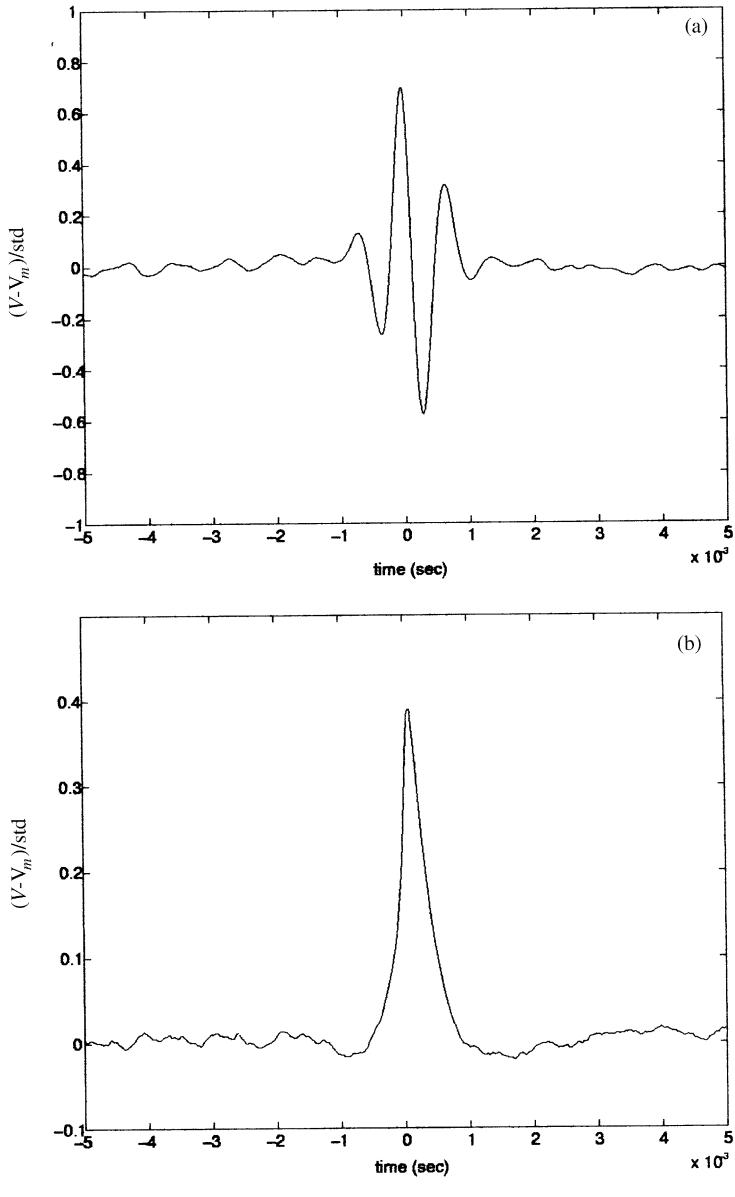

Figure 17. Averaged in-flow velocity time histories conditioned by an reference identification technique [29]: (a) $x/D = 3$; (b) $x/D = 0$.

trigger to the anemometric data itself. It is shown that the region close to the nozzle is dominated by oscillations that correspond to the shear layer instability oscillations observed on the velocity spectra close to the nozzle (see Figure 9(a)). This is the same behavior observed in Figure 13, but with no evidence of the lower frequency event. The shape of the averaged structures at larger distance ($x/D = 10$) is indeed very similar to that found by the acoustic method.

It is therefore possible to argue that the fluid-dynamic events educed from the acoustic method, which are the structures responsible for noise generation within the region

$7 \leqslant x/D \leqslant 9$, have the same physical nature as those educed by the *wavelet* method, i.e., those responsible for turbulence intermittency. It is straightforward to argue that they are the same structures. They should be responsible both for the intermittent behavior of the velocity gradients and, due to their intermittent nature, the noise emission. Further support for this idea is given in the following section.

5.3. WAITING TIME STATISTICS

A statistical analysis of the waiting time between the passage of successive noise-emitting structures has been performed by computing the PDF of the set of time events $\delta t = t_0^i - t_0^{i-1}$, δt being the delay time between successive peaks in the farfield pressure (section 2). This study may be useful in giving more insight into the events selected for the averaging procedure performed above and, in particular, for the evaluation of a possible correlation between them.

In Figure 18(a), the PDF of the waiting time δt is reported for the position $x/D = 3$. The plot is on a semi-log scale, so that the linear trend observed for about $\delta t > 0{\cdot}5 \times 10^{-3}$ s corresponds to an exponential decay. From a physical viewpoint, this indicates that the selected events may be considered statistically independent and uncorrelated with each other [34]. The transition time $\delta t > 0{\cdot}5 \times 10^{-3}$ s corresponds approximately to the period of the shear layer oscillations previously observed (the inverse of the frequency corresponding to the peak of Figure 9(a)), even though this range of δt is not well resolved because of the limited number of events selected for the PDF computation. This result also indicates that the functional form adopted for the time statistics in the numerical validation of the present method (section 3) has physical basis. Furthermore, for time delays larger than the period characterizing the shear layer oscillations, no correlation between events is observed, supporting the idea that the peaks in the pressure fluctuation are related to structures forming at larger distances from the selected position.

The case corresponding to $x/D = 12$ is reported in Figure 18(b). Here, it is observed that a typical time spacing between the structures may be detected and is of the order of 10^{-2} s. For larger time delays, an exponential decay is again observed. This result shows that the time interval of 0·01 s may be considered as the correlation time between structures, since when the waiting times exceed this limit the events become statistically independent. The space length corresponding to this time scale approximately coincides with the integral length of the fluctuating velocity, evaluated by integrating the autocorrelation coefficient [37], and it is of the order of the jet diameter.

Two main results can therefore be argued from this analysis. The first one is that the structures generating noise are intermittent as they are characterized by strongly non-Gaussian and exponential-like time statistics, as is usually observed when the structures responsible for turbulence intermittency are examined [33]. Secondly, such events are large-scale structures with a typical length scale of the order of the integral length, i.e., the jet diameter. The former point gives further support to the idea that structures emitting noise are the same as those responsible for turbulence intermittency. On the other hand, the latter result may be useful for arguing some possible interpretations of the physical nature of such structures. A discussion on this aspect is given in the concluding section.

6. CONCLUDING REMARKS

A conditional averaging technique for the eduction of fluid-dynamic events responsible for farfield noise generation in a low Mach number cold jet flow has been presented. The

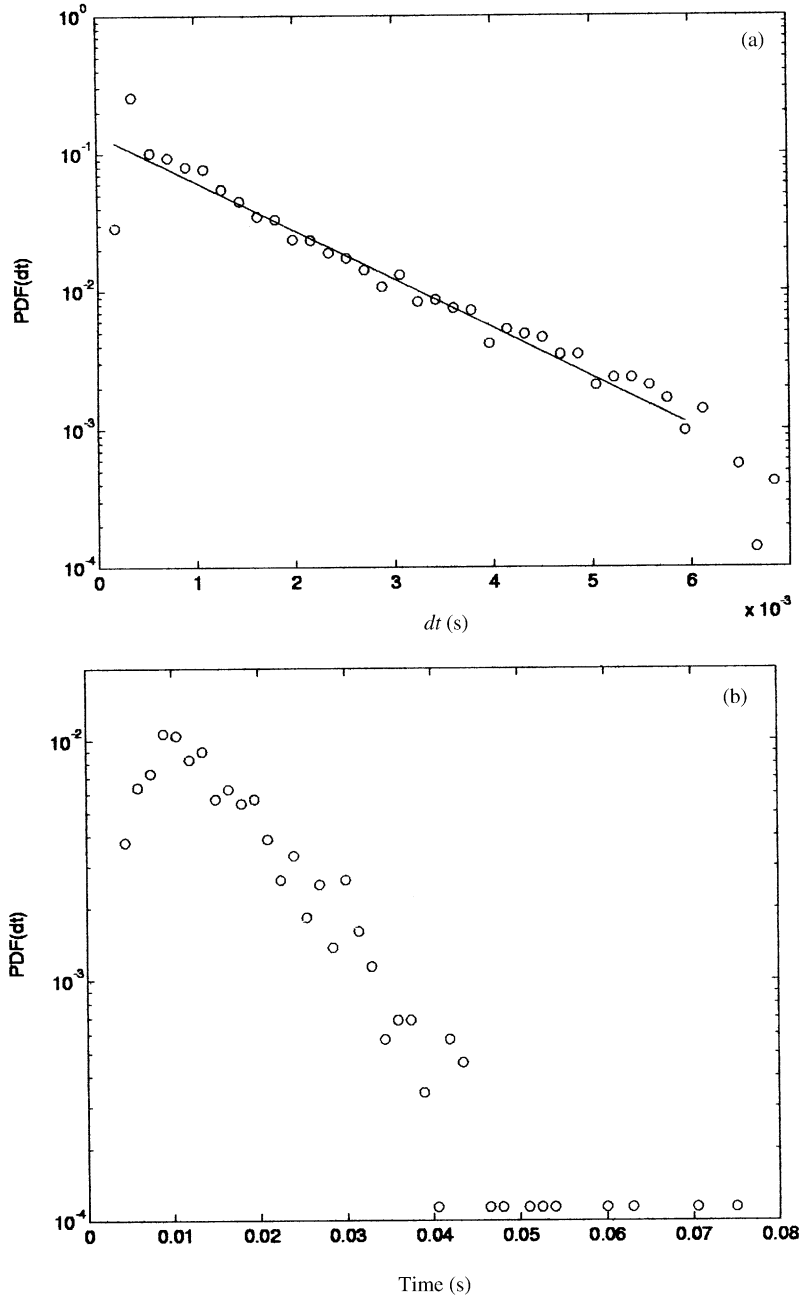

Figure 18. PDF of the waiting time on a semi-log scale: (a) $x/D = 3$; (b) $x/D = 12$. The straight line represents an exponential fit.

main idea is the use of the farfield noise as trigger for a conditional average of the in-flow velocity and pressure, in order to identify velocity or in-flow pressure time histories induced by fluid-dynamic events responsible for the farfield noise. Information about the nature of the structures in the flow responsible for the farfield noise has been extracted, giving some insights into the physics of the system.

The experimental measurements were performed in the flow generated by a free jet which was located in an anechoic chamber where the background noise was minimized and the acoustic environment well controlled. The basic procedure for the conditional averaging has been modelled analytically and validated numerically using a simplified model of the jet flow and of the coherent structures which are treated as finite-length acoustic sources.

The ensemble averages of the velocity and in-low pressure, conditioned on the farfield pressure peaks, have shown that, in addition to the expected effects related to the oscillation of the shear layer in the mixing region close to the nozzle exit (at about $x/D \leqslant 4$), noise generation is strongly affected by fluid-dynamic events forming far downstream. It is observed that for distances $x/D \geqslant 6$, efficient noise sources are structures which induce averaged time signatures of cusp-like form with a significant amplitude which is around 25 and 50% of the velocity and pressure r.m.s. respectively. Moreover, these emitting noise structure are located within the region where the flow is fully turbulent.

The comparison of the averaged signatures with a reference identification method based on the wavelet transform suggests that the structures educed here are, from the physical viewpoint, the same as those responsible for turbulence intermittency.

The statistical analysis of the separation time between successive events indicated that in the region close to the jet exhaust ($0 \leqslant x/D \leqslant 4$), the events are statistically independent, thus suggesting that pressure fluctuations in that region should be related to uncorrelated structures (structures appearing far downstream). When the distance is increased, an increased correlation time has been observed; in terms of spatial separation, this indicated that in the farfield, the noise-generating events are large-scale structures.

These results may help to clarify some topological characteristics of the structures which, accounting also for previous analyses (e.g., the averaged structures found by Lau and Fisher [27], Figure 8), are argued to be ring vortices forming in the turbulent region of the jet flow. Indeed, when a moving ring vortex approaches the anemometric probe placed on the jet axis, it induces an increase in the longitudinal velocity, which peaks when the ring vortex is at the same x/D as the probe, and then decreases, Thus, the overall signature on the longitudinal velocity has a cusp-like shape as the ones observed in the present work. It is also well known that such structures are highly unstable far from the nozzle, and this might explain their intermittent nature and duration. However, topological details cannot be clarified by the present analysis, so that idea that analogous effects might be produced by vortex interactions (such as vortex pairing) cannot be disregarded. Further analyses, e.g., with multiprobe anemometry and flow-field visualizations or measurement techniques (such as Particle Image Velocimetry) might be useful to clarify this last point, and to give more information on the topological properties of such structures.

Apart from topological aspects, the main feature observed in the present experiment is that by changing the position of the in-flow probes, the time delay of the averaged structures varies significantly and, accounting for the local convection velocity and the sound propagation velocity, the spatial location of the events producing noise (whatever they physically are) is instead nearly constant and contained within the region $7 \leqslant x/D \leqslant 9$, in agreement with results obtained by Shaffar [23] at much larger Mach number, using the casuality method. From a statistical viewpoint, it is found therefore that the region where the events emitting noise are located, belongs to the turbulent region of the jet flow rather than to the near region as was extensively observed in previous studies. To this extent, it should be stressed that most of the methods adopted so far for the determination of the noise-producing region in jet flows were based on the spectral analysis of the farfield pressure signals or on the computation of farfield *SPL*. These estimators are dominated by

acoustic effects generated from the region close to the nozzle exit since they contain strong periodic or quasi-periodic contributions which are retrieved efficiently by the Fourier analysis. Present results indicate instead that a significant part of the farfield noise is generated in the fully turbulent region of the jet as an effect of unsteady highly energetic fluid-dynamic structures. The difficulty in correlating this idea with previous studies based mostly on standard Fourier analyses lies in the observation that such structures are unsteady and localized in time. Their effect is therefore completely missed by the Fourier decomposition, since their energy is distributed over the whole time domain by the projection of the signal onto the trigonometric basis which is (theoretically) infinitely extended. Indeed, even if a time-localized event cannot be observed by the overall farfield spectrum, this does not mean that it cannot emit noise, and present analysis shows that its acoustic contribution is relevant. More detailed information could be achieved by the use of post-processing methods more suitable to identify localized events (such as by means of wavelets transform). In this way, it should be possible to understand which is the actual contribution of the intermittent structures to the farfield *SPL*. This is a non-trivial pursuit and it is the task for future works currently undertaken by the authors.

ACKNOWLEDGMENTS

The authors gratefully acknowledge the assistance of ISPESL (Dr Lenzuni in particular) in providing access to the anechoic chamber and S. Conforto, T. D'Alessio, S. Sciuto for assistance in data acquisition. M. Bosi is also acknowledged for the continuous support during the experimental work. M. C. acknowledges the financial support of the Italian Ministry of Foreign Affairs under an Italian–Irish exchange scheme.

REFERENCES

1. M. J. Lighthill 1952 *Proceedings of the Royal Society of London A* **211**, 564–587. On sound generated aerodynamically. I: general theory.
2. A. Powell 1964 *Journal of the Acoustic Society of America* **36**, 177–195. Theory of vortex sound.
3. A. Powell 1995 *Transactions of the American Society of Mechanical Engineers* **117**, 252–260. Why do vortices generate sound?
4. W. Möhring 1978 *Journal of fluid Mechanics* **85**, 685–691. On vortex sound at low Mach number.
5. A. Powell 1995 *Journal of the Acoustic Society of America* **97**, 1534–1537. Vortex sound theory: direct proof of equivalent of "vortex force" and "vorticity alone" formulations.
6. T. Kambe 1986 *Journal of Fluid Mechanics* **173**, 643–666. Acoustic emissions by vortex motions.
7. C. K. W. Tam 1995 in *Aeroacoustics of Flight Vehicles* (H. H. Hubbard editor). Jet noise generated by large scale coherent motion. Acoustical Society of America.
8. C. J. Moore 1977 *Journal of Fluid Mechanics* **80**, 321–367. The role of shear layer instability waves in jet exhaust noise.
9. S. C. Crow and F. H. Champagne 1971 *Journal of Fluid Mechanics* **48**, 547–591. Orderly structures in jet turbulence.
10. P. Bradshaw, D. H. Ferriss and R. F. Johnson 1964 *Journal of Fluid Mechanics* **19**, 591–624. Turbulence in the noise-production region of a circular jet.
11. A. J. Yule 1978 *Journal of fluid Mechanics* **89**, 413–432. Large-scale structure in the mixing layer of a round jet.
12. W. Rodi 1975 in *Studies in Convection*, (B. Launder, editor), (pp. 79–165). A review of experimental data of uniform density free turbulent boundary layers. New York: Academic Press.
13. J. Laufer, R. E. Kaplan and W. T. Chu 1973 *AGARD CP 131 on Noise Mechanisms*. On the generation of jet noise.

14. J. E. Ffowcs Williams and A. J. Kempton 1978 *Journal of Fluid Mechanics* **84**, 673–694. The noise from the large scale structure of a jet.
15. R. Verzicco, A. Iafrati, G. Riccardi and M. Fatica 1997 *Journal of Sound and Vibration* **200**, 347–358. Analysis of the sound generated by the pairing of two axisymmetric co-rotating vortex rings.
16. A. K. M. F. Hussain 1983 *Physics of Fluids* **26**, 2816–2850. Coherent structure—reality and myth.
17. J. E. Bridges and A. K. M. F. Hussain 1986 *Bulletin of the American Physical Society* **31**, 1684–1690. Measurements concerning vertex pairing as a noise source in turbulent jets.
18. M. J. Fisher, M. Harper-Bourne and S. A. L. Glegg 1977 *Journal of Sound and Vibration* **51**, 23–54. Jet engine noise source location: the polar correlation technique.
19. H. K. Lee and H. S. Ribner 1972 *Journal of the Acoustic Society of America* **52**, 1280–1290. Direct correlation of noise and flow of a jet.
20. J. E. Siddon 1973 *AGARD CP* 131 *on Noise Mechanisms*. Noise source diagnostics using casuality correlation.
21. W. C. Meecham and P. M. Hurdle 1973 *AGARD CP* 131 *on Noise Mechanisms*. Use of cross-correlation measurements to investigate noise generating regions of a real jet engine and a model jet.
22. M. Shaffer 1979 *Journal of Sound and Vibration* **64**, 73–83. Direct measurements of the correlation between axial in-jet velocity fluctuations and far field noise near the axis of a cold jet.
23. J. Billingsley and R. Kinns 1976 *Journal of Sound and Vibration* **48**, 485–510. The acoustic telescope.
24. S. K. Tang and N. W. M. Ko 1993 *American society of Mechanical Engineers, Journal of Fluids and* Engineering **115**, 425–435. A study on the noise generation mechanism in a circular air jet.
25. D. Juvé, M. Sunyach and G. Comte-Bellot 1980 *Journal of Sound and Vibration* **71**, 319–332. Intermittency of the noise emission in subsonic cold jets.
26. M. Lesieur 1990 *Turbulence in Fluids*. Dordrecht: Kluwer; second edition.
27. J. C. Lau and M. J. Fisher 1975 *Journal of Fluid Mechanics* **67**, 299–337. The vortex-street structure of 'turbulent' jets.
28. R. Camussi and G. Guj 1999. *Physics of Fluids* **11**, 423–431. Experimental analysis of intermittent coherent structures in the near field of a high *Re* turbulent jet flow.
29. R. Camussi and G. Guj 1997 *Journal of Fluid Mechanics* **348**, 177–199. Orthnormal wavelet decomposition of turbulent flows: intermittency and coherent structures.
30. C. Baudet, S. Ciliberto and J. F. Pinton 1991 *Physical Review Letters* **67**, 193–195. Spectral analysis of the Von Karman flow using ultrasound scattering.
31. C. Baudet, O. Michel and W. J. Williams 1999 *Physica D* **128**, 1–17. Detection of coherent vorticity structures using time-scale resolved acoustic spectroscopy.
32. P. Abry, S. Fauve, P. Flandrin and C. Laroche 1994 *Journal of Physics II (France)* **4**, 725–733. Analysis of pressure fluctuations in swirling turbulent flows.
33. E. Villermaux, B. Sixou and Y. Gagne 1995 *Physics of fluids* **7**, 2008–2013. Intense vortical structures in grid-generated turbulence.
34. G. Guj and R. Camussi 1999 *Journal of Fluid Mechanics* **382**, 1–26. Statistical analysis of local turbulent energy fluctuations.
35. R. Camussi and R. Verzicco 2000 *Physics of Fluids* **12**, 676–687. Anomalous scaling exponents and coherent structures in high *Re* fluid turbulence.
36. P. M. Morse and K. U. Ingard 1968 *Theoretical Acoustics*. New York: McGraw-Hill.
37 J. Hinze 1976 *Turbulence*. New York: McGraw-Hill; second edition.
38. K. B. M. Q. Zaman and A. K. M. F. Hussain 1984 *Journal of Fluid Mechanics* **138**, 325–351. Natural large-scale structures in the axisymmetric mixing layer.
39. H. S. Ribener 1981 *American Institute of Aeronautics and Astronautics Journal* **19**, 1513–1524. Perspective on jet noise.
40. I. Wygnanski and H. Fiedler 1969 *Journal of Fluid Mechanics* **38**, 3–45. Some measurements in the self-preserving.
41. H. Schlighting 1979 *Boundary Layer Theory*. New York: McGraw Hill.
42. B. J. Cantwell 1990 *Annual Review of Fluid Mechanics* **13**, 457–515. Organized motion in turbulent flow.